thermo

MDPI

Article

Advancing Sustainable Refrigeration: In-Depth Analysis and Application of Air Cycle Technologies

Lorenz Hammerschmidt [1,*], Zlatko Raonic [1] and Michael Tielsch [2]

[1] Department of Environmental and Energy Process Engineering, Technical University of Leoben, 8700 Leoben, Austria; zlatko.raonic@unileoben.ac.at
[2] Christof Systems GmbH, 8051 Graz, Austria
* Correspondence: lorenz.hammerschmidt@me.com

Abstract

Air cycle systems, once largely replaced by vapour-compression technologies due to efficiency concerns, are now re-emerging as a viable and sustainable alternative for highly dynamic thermal applications and excel in ultra-low temperature. By using air as the working fluid, these systems eliminate the need for synthetic refrigerants and comply naturally with evolving environmental regulations. This study presents the conceptual design and simulation-based analysis of a novel air cycle machine developed for advanced automotive testing environments. The system is intended to replicate a wide range of climatic conditions—from deep winter to peak summer—through the use of fast-responding turbomachinery and a flexible control strategy. A central focus is placed on the radial turbine, which is designed and evaluated using a modular, open source framework that integrates geometry generation, off-design CFD simulation, and performance mapping. The study outlines a potential operating strategy based on these simulations and discusses a control architecture combining lookup tables with zone-specific PID tuning. While the results are theoretical, they demonstrate the feasibility and flexibility of the proposed approach, particularly the turbine's role within the system.

Keywords: air-cycle; turbomachinery; sustainability; automotive; air conditioning

check for updates

Academic Editor: Salvatore Vasta

Received: 6 September 2025
Revised: 24 October 2025
Accepted: 31 October 2025
Published: 12 November 2025

Citation: Hammerschmidt, L.; Raonic, Z.; Tielsch, M. Advancing Sustainable Refrigeration: In-Depth Analysis and Application of Air Cycle Technologies. *Thermo* **2025**, *5*, 52. https://doi.org/10.3390/thermo5040052

Copyright: © 2025 by the authors. Licensee MDPI, Basel, Switzerland. This article is an open access article distributed under the terms and conditions of the Creative Commons Attribution (CC BY) license (https://creativecommons.org/licenses/by/4.0/).

1. Introduction

The transportation sector accounts for approximately 25% of greenhouse gas emissions in the European Union [1], and increasing attention is now being paid to non-exhaust pollutants such as brake and tyre wear particles. These fine particulates (PM2.5 and PM10) pose serious health risks, particularly in urban environments where braking is frequent [2–4]. To address these challenges, the upcoming Euro 7 regulation and the United Nations Global Technical Regulation (UN GTR) propose stricter limits on brake wear and tyre abrasion emissions [5–7]. As part of this regulatory framework, the World-harmonized Light-duty Vehicles Test Procedure for Brakes (WLTP-B) has been introduced to provide more representative and harmonised testing conditions.

Achieving accurate and repeatable emission measurements under such procedures requires a testing infrastructure capable of simulating dynamic real-world conditions. However, conventional thermal conditioning systems often lack the responsiveness and flexibility needed to replicate transient temperature and pressure profiles typical of on-road scenarios. To address this gap, this study introduces a novel air-based conditioning system, built around an air cycle architecture. By using air as the working fluid and leveraging

fast-response turbomachinery, the system enables rapid thermal transitions and pressure control without the inertia associated with traditional refrigerant-based systems.

A key contribution of this work is the detailed design and simulation-based evaluation of the system's radial turbine—the core energy conversion component. While commercial data are available for most other components, the turbine is designed from scratch using pyTurbo, an in-house developed, open source design framework. The study focuses on the off-design performance of the turbine, its role within the system, and the development of a flexible operating strategy based on CFD analysis. The goal is to explore the feasibility of using air cycle machines for highly dynamic automotive test environments and to demonstrate the application of an integrated design and control methodology for future test bench infrastructure.

2. Methodology

2.1. WLTP-B

The test system of the WLTP-B consists of four major subsystems, namely a climatic conditioning unit, the brake enclosure, the sampling unit, and the exhaust. The system can be designed as a closed- or open-loop system. The latter requires a fan in the exhaust to ensure negative pressure inside the piping system. A simplified flow schematic of the system can be seen in Figure 1. Similarly to the WLTP, the environmental conditions are fixed and prescribed at 23 °C and a relative humidity of 50%. However, research has shown that testing environments—particularly temperature, airflow velocity, and humidity—strongly influence WLTP-B outcomes, with a significant variability observed under real-world driving conditions [8]. While exhaust emissions are commonly evaluated using Real Driving Emission (RDE) protocols, brake emissions are still predominantly assessed on dynamometers under constant and often unrealistic environmental conditions. However, previous studies [9–12] underline the importance of replicating dynamic real-life scenarios to ensure more representative and robust emission measurements.

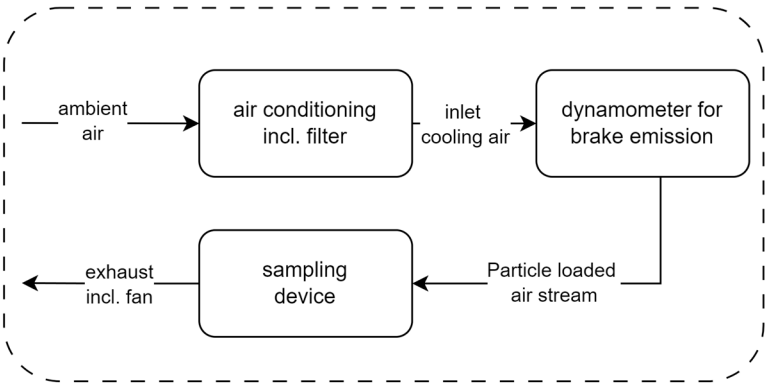


Figure 1. Open-loop schematic of a brake emission test facility. Adapted from [13].

To address this gap, the present study introduces an air-based conditioning system designed to enhance the test bench's ability to simulate realistic thermal and pressure profiles. Unlike conventional fluid-based refrigeration systems, which are characterised by high thermal inertia and slow response times, the air-based system enables a rapid modulation of inlet air parameters. The system can be seamlessly integrated into the standard WLTP-B testing environment, substituting the conventional air conditioning system.

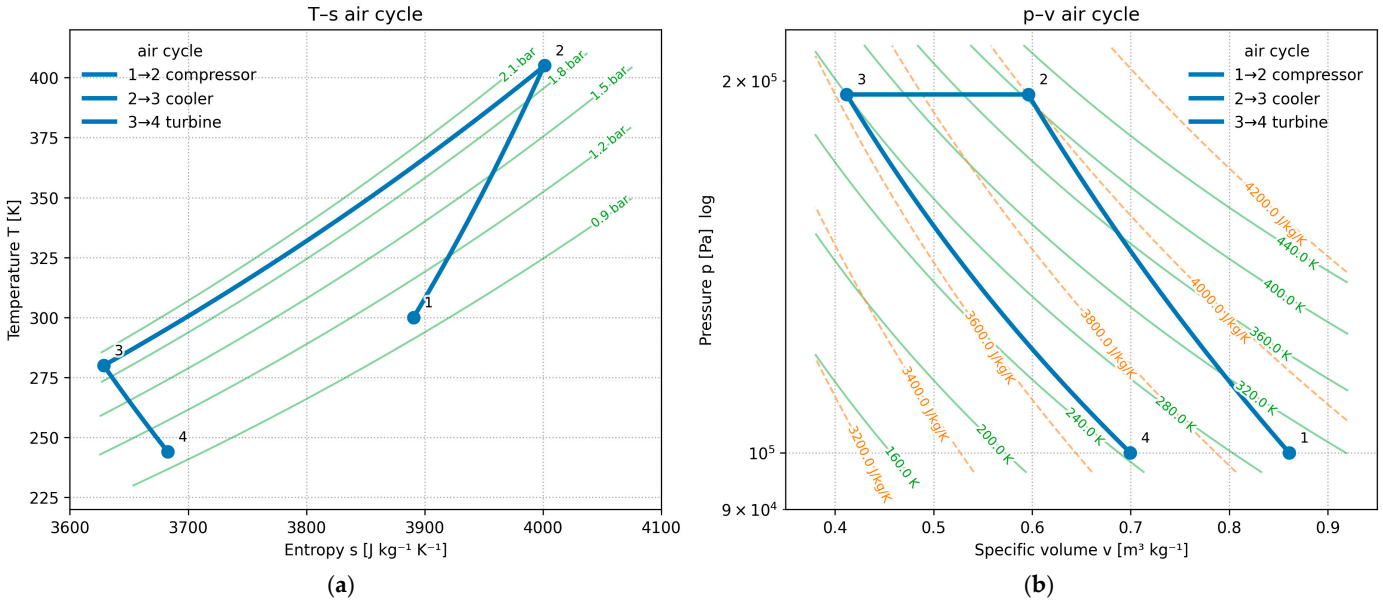
To support an extended testing range—including varying inlet temperatures, pressures, and transient events—the entire test bench infrastructure must offer fast and accurate response capabilities. Conventional refrigerant systems, often relying on large thermal fluid volumes, exhibit high inertia and are poorly suited for dynamic operation. In contrast,

air cycle systems provide a compact, responsive alternative that enables a rapid modulation of test conditions without major modifications to existing facilities.

2.2. Christof Air Cycle

The air cycle is effectively approximated by a reversed Brayton cycle. It consists of compression, near-isobaric cooling in a heat exchanger, and expansion. The configuration considered here is open: ambient air is compressed from about 1 bar to approximately 2 bar_{abs}, rejects heat at nearly constant pressure in the cooler, and then expands through a turbine back to ambient pressure.

Compression and expansion are modelled as polytropic processes with exponents n_c and n_t, respectively, obtained from the measured end states or from specified efficiencies. Because compression raises the air temperature, the cooler lowers the turbine inlet temperature to increase the net specific cooling effect. Figure 2 shows the T–s and p–v diagrams of the cycle at full load. The working fluid is treated as dry air with zero humidity, and pressure drops outside the turbomachinery are neglected.



(**a**) (**b**)

Figure 2. (**a**) T-s and (**b**) p-V diagram of the Christof Air Cycle.

Similarly to other refrigeration systems, the Coefficient of Performance (COP) can be calculated as follows:

$$\mathrm{COP} = \frac{\mathrm{Q_L}}{W_{net,in}} = \frac{h_1 - h_4}{\underbrace{(h_2 - h_1)}_{P_{compressor}} - \underbrace{(h_3 - h_4)}_{P_{Turbine}}} \tag{1}$$

The Christof Air Cycle was developed to meet these requirements and replicate realistic testing scenarios—including rapid ambient temperature shifts, thermal transients, and pressure fluctuations. By using air as the working fluid and eliminating phase-change processes, the system avoids the thermal delays inherent to vapour compression refrigeration systems (VCRSs). This allows the air cycle to achieve significantly faster thermal response and greater flexibility in test bench integration. Furthermore, they eliminate concerns related to high global warming potential (GWP), toxicity, or flammability of conventional refrigerants.

The Christof Air Cycle represents a novel approach tailored to meet the evolving demands of the automotive testing industry [14,15]. It provides precise control across a

broad range of operating conditions and is designed for installation near the test intake, thereby reducing ducting losses and thermal lag. System regulation is achieved through coordinated adjustment of the compressor and turbine rotational speeds, in combination with partial or complete bypassing of system components. A sophisticated control system enables rapid transitions between different operating points.

Although the initial investment is higher due to specialised components and the relative novelty of air cycle technology, operational and total lifecycle costs may be lower compared to conventional VCRSs. The air cycle system offers a significantly wider operational range, enabling the execution of more complex and variable test cycles. These cycles tend to be shorter, and regeneration times between tests are greatly reduced, which contributes to increased overall efficiency and throughput for testing facilities.

Figure 3 illustrates the system architecture, highlighting the major components and their configuration. A flow controller dynamically adjusts compressor speed to ensure a constant mass flow under varying pressure conditions. The outlet temperature influences both the valve positions of the chiller and turbine, as well as the turbine's rotational speed, allowing for the tightly coupled control of system parameters in response to target test profiles.

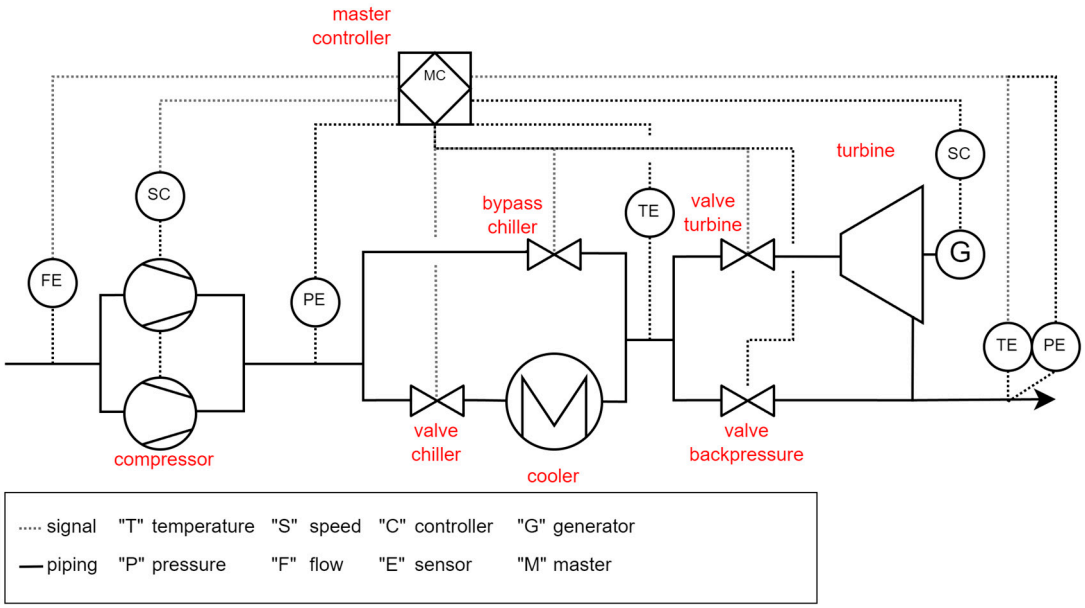


Figure 3. Schematic of the main components and controllers of the Christof Air Cycle.

2.3. Components

2.3.1. Valve

Valves play a critical role in regulating pressure, mass flow, and temperature within the air cycle system. By throttling or diverting airflow through different branches, they enable the precise control of turbine inlet temperature and overall system backpressure. In this setup, butterfly valves are employed due to their compact geometry, low pressure drop when fully open, and fast actuation, which make them ideal for dynamic air cycle operation.

The actual relationship between the valve opening angle and mass flow is highly nonlinear, particularly for butterfly valves. Small opening angles already cause a large change in effective flow area, while further opening produces only marginal increases in flow. This behaviour can destabilise control loops if the controller assumes a linear relationship between the control signal and throughput. To counteract this, the control system applies a valve linearisation based on experimentally determined flow data. The base dataset consists of measured through-flow values, $\dot{V}_{norm}(x)$, at discrete valve openings, x, converted to a

normalised scale. From this curve, an inverse mapping, $x_{lin} = f^{-1}\left(\dot{V}_{\text{norm}}\right)$, is derived, which defines the non-linear actuation profile required to achieve a linear flow response with respect to the control signal.

Figure 4b visualises this process. The grey curve represents the measured non-linear flow characteristic of the butterfly valve when actuated with a linear opening signal. The blue line shows the corresponding compensatory valve position required to obtain a linearised flow. The orange curve confirms the result—the effective air flow increases linearly with the control signal, providing a uniform control response across the operating range.

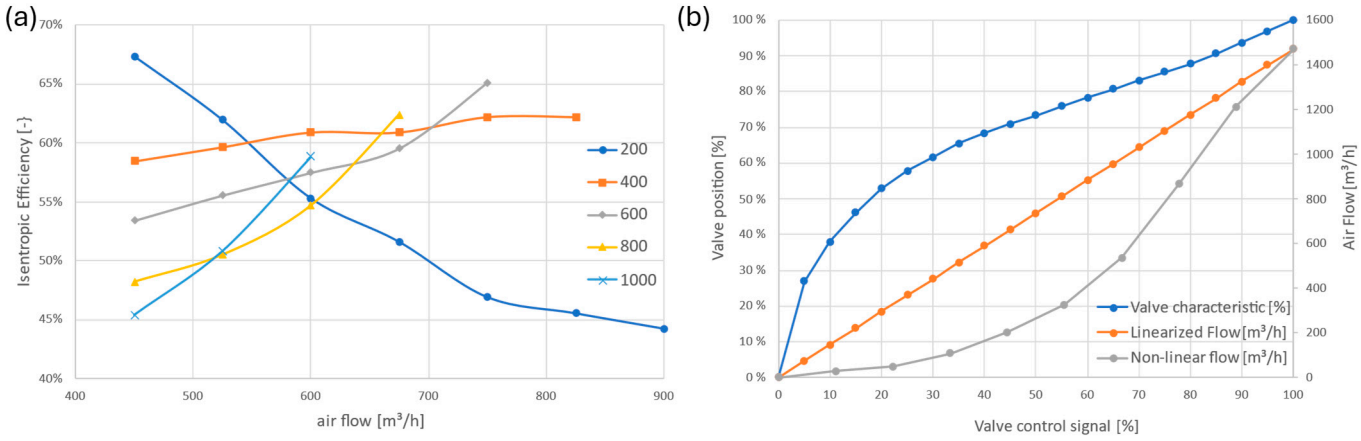


Figure 4. (**a**) Efficiency map of the compressor Airtech AKB1000. (**b**) Valve linearization.

Within the air cycle, the chiller valve and bypass valve jointly control the turbine inlet temperature by distributing the total mass flow between the cooling branch and the bypass duct. The turbine valve and backpressure valve govern the expansion ratio and mass flow through the turbine, thereby determining the cooling effect due to expansion. Finally, the primer valve fine-tunes the system pressure and stabilises transient operation, ensuring that the required pressure level is maintained during fast load changes.

2.3.2. Compressor

The air cycle utilises a side-channel compressor, specifically the Airtech AKB1000 (AIRTECH Group, Rutherford, NJ, USA) [16], which is well-suited for applications requiring moderate pressure increases and high volumetric throughput. The operation field is depicted in Figure 4a. This oil-free blower ensures clean, particle-free air—essential for brake emission testing. Side-channel compressors generate a continuous, pulsation-free flow and tolerate wide operating conditions with relatively low maintenance requirements.

To enhance reliability and scalability, two identical compressors are installed in parallel. This parallel arrangement provides operational redundancy and allows for partial-load operation during lower demand, improving overall energy efficiency. It also enables smoother transitions between operating points by staggering or independently modulating the compressor speeds.

2.3.3. Heat Exchanger

A compact finned-tube air-to-liquid heat exchanger cools the process air while adding only minimal hydraulic resistance. In the system model and performance discussion, the air-side pressure drop across the chiller is assumed to be negligible compared with the overall system pressure losses, so its contribution to the compressor operating point and mass flow control is ignored. Cooling performance is largely decoupled from airflow within the relevant range of operating conditions, which provides a stable and predictable temperature reduction for turbine inlet control.

Because the test bench operates as an open loop, ambient moisture enters the system with the intake air. The pressure rise upstream shifts the dew point to higher temperatures. By cooling the compressed air in the heat exchanger below this dew point, water condenses and can be removed by the downstream separator. This pre-conditioning step reduces humidity before expansion and mirrors established practice in industrial compressed-air treatment [14,15].

2.3.4. Radial Turbine

For the air conditioning unit that is designed and manufactured during this project, the choice for a radial turbine over an axial turbine was evident. From the manufacturing point of view, a radial impeller can be fabricated as one piece either by casting or milling, whereas an axial turbine often demands a separate runner, blades, and casing. Furthermore, the radial turbine can be more compact, a factor often required for small-scale applications such as the air cycle. A radial turbine can deliver more power per unit mass flow and allows a higher pressure ratio without the need for multiple stages. The reason for this can be observed by inspecting one of the most fundamental equations in turbomachinery, the Euler turbomachinery equation, which describes the work as follows:

$$W_x = U_4 C_{\theta 4} - U_6 C_{\theta 6} \tag{2}$$

A radial turbine provides a compact and efficient means to convert the pressure potential of the compressed air into shaft work, which lowers the air temperature through expansion. The stage comprises a stator that accelerates and turns the flow, a rotor that extracts work, and a diffuser that recovers kinetic energy into static pressure. The stator includes a volute—responsible for distributing the air circumferentially—and a row of stator blades, which accelerate and turn the flow to align with the leading edge of the rotor blades. The volute is constructed as a scroll to account for the decreasing mass flow rate along the circumferential direction.

2.4. Design and Analysis—Radial Turbine

The geometry of the turbine was generated using a custom-built framework developed for this research. It integrates a preliminary design module, based on Aungier's methodology [17], with a fully three-dimensional modeller. The modelling environment is entirely Python-based (v.3.10.12), combining the NURBS-based CAD kernel—pyNURBS (v1.0)—with the parametric turbomachinery modeller pyTurbo [18], which provides interfaces to various meshing and optimisation tools. The software was validated against the well-known APU test case [18].

2.4.1. Geometric Modelling—pyTurbo

Unlike other open source turbomachinery modelling solutions, pyTurbo supports geometric intersections while preserving the parametric definition of the geometry. The intersection capability relies on a two-stage algorithm. The primary stage is based on the Projected Polyhedron Algorithm (PPA) developed by Patrikalakis et al. [19,20], which identifies characteristic intersection points. From these, the intersection curve is traced using an iterative marching method at the parametric level.

This functionality is particularly crucial during the volute design process. The volute construction follows a modular structure, allowing for a precise control over both the shape and the flow characteristics at each design step. As shown in Figure 5, the volute consists of key elements: a cross-sectional profile (a), an area function (b) that prescribes the cross-sectional area in the circumferential direction, an inlet stud (d), and the tongue (e), where the base volute (c) intersects with the inlet, forming a distinct boundary.

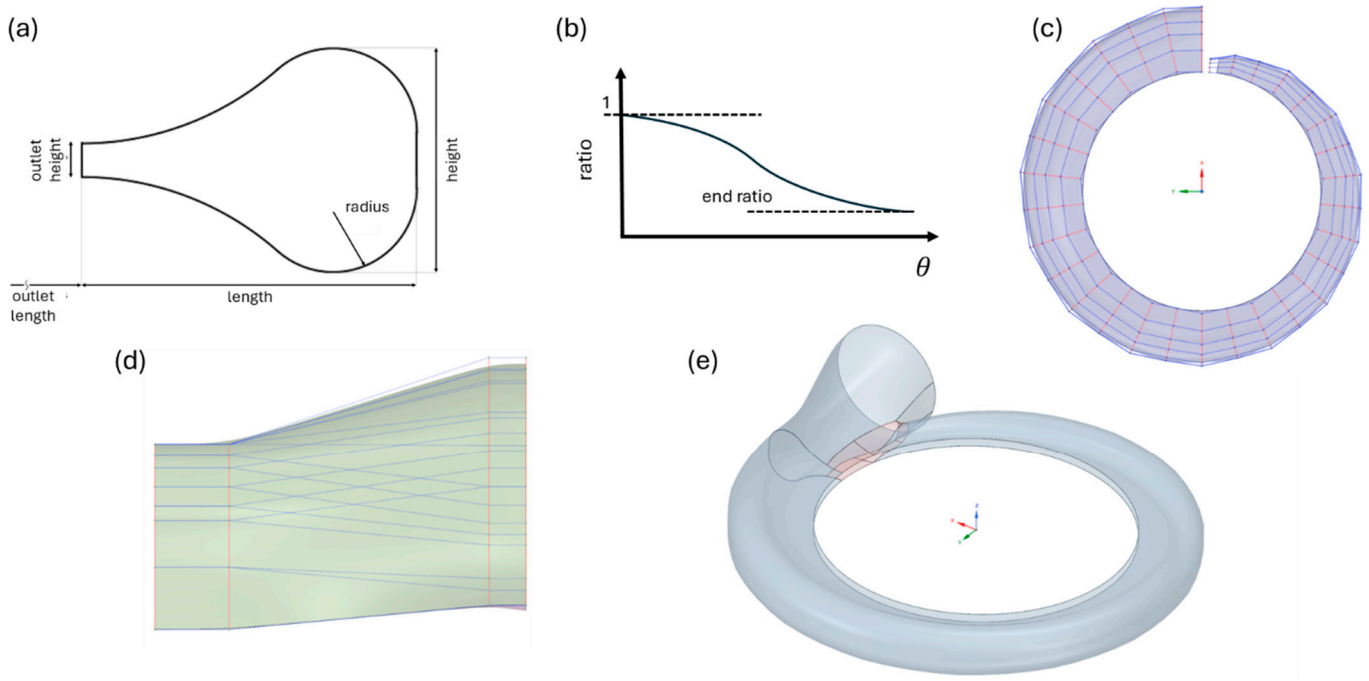


Figure 5. Volute generation sub steps: (**a**) cross-section, (**b**) area function, (**c**) base volute, (**d**) inlet stud, (**e**) volute including tongue.

The base volute is constructed by rotating the cross-sectional profile along the circumferential direction, while gradually reducing its size according to the prescribed area function. Continuity conditions are maintained throughout to ensure a smooth geometric transition. The use of NURBS surfaces allows the creation of the required circular outlet shape by strategically placing weighted control points.

Parts of the volute and the inlet stub are offset relative to each other and then intersected to form the tongue region. The resulting gap at the intersection is closed with a fillet surface, which is carefully designed to meet positional and tangential continuity requirements. This approach ensures a smooth and seamless connection between all adjacent surfaces and preserves the aerodynamic integrity of the design.

2.4.2. Off-Design Analysis and Stability Assessment

Off-design performance plays a critical role in turbomachinery design, especially for machines intended to operate under varying load conditions. While a turbine may be optimised for peak efficiency at a single design point, real-world applications—such as air cycles—require a broad and robust operating field. Deviations from ideal flow conditions can lead to undesirable effects including increased aerodynamic losses, flow separation, unsteady loading, or even local vibrations and thermal stresses that may compromise mechanical integrity.

Compared to compressors, turbines are generally less susceptible to global instabilities such as surge or rotating stall due to the favourable pressure gradient in their flow passages. However, even turbines may exhibit local off-design effects such as boundary layer separation, recirculation, or backflow zones when operating far from their design point. These flow anomalies can induce blade vibrations, fluctuating loads, and contribute to noise, especially when occurring near tip regions or at partial admission conditions [21]. Such unsteady flow phenomena can lead to increased stress on bearings, seals, and blade roots.

To assess off-design behaviour systematically, several modelling strategies are available. In the conceptual stage, one-dimensional mean-line [22] or streamline-curvature methods provide rapid performance estimates across a wide operating field. These are typ-

ically followed by CFD simulations, where steady-state RANS solvers with circumferential averaging (e.g., the mixing-plane method) are employed to capture rotor–stator interactions at moderate computational cost [18,23–25]. For periodic unsteadiness, harmonic balance techniques [26–28] offer a frequency-domain alternative to transient simulations, efficiently capturing dominant oscillatory behaviour. For stress and vibration analysis under off-design loading, fluid–structure interaction methods coupling CFD and FEM are used to identify critical structural responses [29–31].

In this study, the off-design performance of the radial turbine is analysed by varying rotational speed and inlet total pressure, which are controlled via the electric drive and upstream compressor. The turbine features fixed geometry without variable guide vanes [32–34]. For each operating point, a steady CFD simulation using the mixing-plane approach is performed. The resulting data yields performance metrics such as isentropic efficiency, pressure ratio, and corrected mass flow, which are assembled into performance maps. These maps visualise the turbine's behaviour over a wide range of speeds and expansion ratios, enabling the identification of optimal and safe operating zones.

Beyond performance maps, further indicators are required to assess the stability of a given operating point. Key diagnostics include solver convergence behaviour—where smooth residual decay and stable pressure distributions suggest flow regularity—as well as inspection of flow fields. Stable operating points are typically characterised by attached boundary layers, minimal recirculation, and monotonic blade loading. In contrast, unstable points exhibit flow separation, unsteady wakes, or pressure fluctuations along the blade surface. Evaluating these fields allows the identification of undesirable regions within the operating envelope, where efficiency drops or component stress may become unacceptable. Together, this multi-layered analysis ensures that the turbine delivers not only high efficiency, but also robust performance under the off-design conditions expected in real-world operation.

The turbine efficiency was calculated using the total values at the inlet and static values at the outlet, resulting in the total static efficiency:

$$\eta_{ts} = \frac{1 - T_{03}/T_{01}}{1 - \left(\frac{p_3}{p_{01}}\right)^{\frac{\kappa-1}{\kappa}}} \tag{3}$$

3. Results

3.1. Oprationsfield—Radial Turbine

The base design of the radial turbine was developed using an in-house mean-line design tool, based on the nominal design parameters listed in Table 1. The initial design of the turbine is optimised towards the design point and tested at various off-design points. Geometry generation was carried out using pyTurbo (v1.0), while the meshing of the rotor and stator was performed in Ansys TurboGrid. The volute was separately meshed using Ansys Meshing.

Table 1. Design parameters of Christof Air Cycle.

Parameter	Value	Unit
Air flow	0.44	kg s^{-1}
Total inlet pressure	195,000	Pa
Total inlet temperature	280	K
Outlet pressure	90,000	Pa
Rotational speed	25,000	rpm

All simulations were carried out in Ansys CFX (v2022 R2) using a steady-state RANS solver. A mixing-plane interface was applied between the stator and rotor, and between the volute and stator. The boundary conditions (Table 1) included the total pressure and total temperature at the inlet, static pressure at the outlet, and zero humidity. The turbine's off-design behaviour was evaluated by systematically varying two key parameters: the inlet total pressure (from 1.15 bar to 1.95 bar_{abs}) and the rotational speed (from 2500 rpm to 21,000 rpm). These variations were used to generate a performance map for the machine. Turbulence was modelled using the k-ω SST model. All simulations were slowly ramped up before reaching the boundary conditions to avoid shock formations and oscillations inside the simulation domain. For the design point, a mesh independency was ensured by testing three different mesh qualities. Throughout the domain, a y^+ of below 5 is achieved.

Figure 6a shows the power output over the pressure range, while Figure 6b provides the efficiency over the same range. The power can be directly related to the work extracted from the system, while the efficiency map provides insights on stability and optimal conditions. With the combination of the power output and the efficiency over the pressure ratio, the operation set-points of the turbine can be set. The maps indicate that, for each speed line, there exists a local maximum efficiency, often associated with moderate pressure ratios. At higher speeds, both power output and peak efficiency increase; however, operating too far from the design point (either at low speeds or very low pressure ratios) results in a significant efficiency loss. This trend reflects increasing aerodynamic losses due to flow separation and misaligned incidence. Figure 6a shows power rising with the pressure ratio at a constant rotational speed, as predicted by $P \approx \dot{m}\,\eta_t\,c_p T_{01}\left(1-\pi^{-(\kappa-1)/\kappa}\right)$; the near-linear appearance over $\pi = 1.1$–1.9 reflects the weak curvature of the isentropic work in this range, while the small deviations match the efficiency peaks observed in Figure 6b. The steeper slopes at higher rotational speeds are expected because both the blade-tip speed $u \propto N$ and swallowing capacity rise, so $P \propto \dot{m}\,u\,\Delta C_\theta$ increases with N.

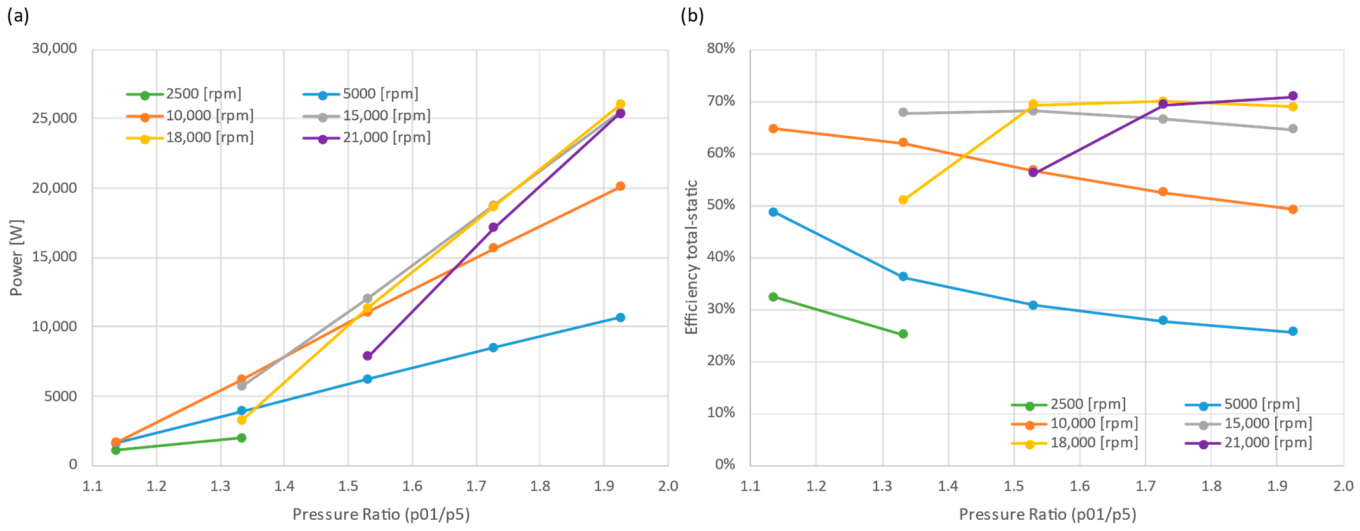


Figure 6. Efficiency map for the radial turbine. (**a**) Power output vs. pressure drop. (**b**) Turbine efficiency vs. pressure drop.

To assess the underlying flow phenomena, velocity fields at different operating points were evaluated. Figure 7 compares the velocity distribution through the stator and rotor passages at two operating points, 18,000 rpm (a) and 10,000 rpm (b), both at 1.35 bar inlet pressure. At the higher rotational speed, the lower pressure ratio results in a mismatch between the incoming flow and the rotor blade angles. The resulting high incidence at

the leading edge causes early flow separation on the pressure side of the rotor blade. This separation region extends across the blade passage, forming a recirculation zone that moves from the pressure to the suction side. When the rotational speed is reduced to 10,000 rpm, the velocity triangles at the stator–rotor interface realign, resulting in a better incidence and a more uniform flow. Under these conditions, the separation zone vanishes, and the flow remains well attached throughout the passage. This observation corresponds directly with the performance trends shown in Figure 6. Despite the lower shaft speed, the improved internal flow structure at 10,000 rpm leads to a higher total power output and better efficiency at this pressure level. In contrast, the increased aerodynamic losses at 18,000 rpm offset the potential benefit of higher blade speed. These findings highlight the importance of matching the operating point to the available boundary conditions. Even at reduced speeds, the performance can be optimised by avoiding off-design effects such as incidence mismatch and separation.

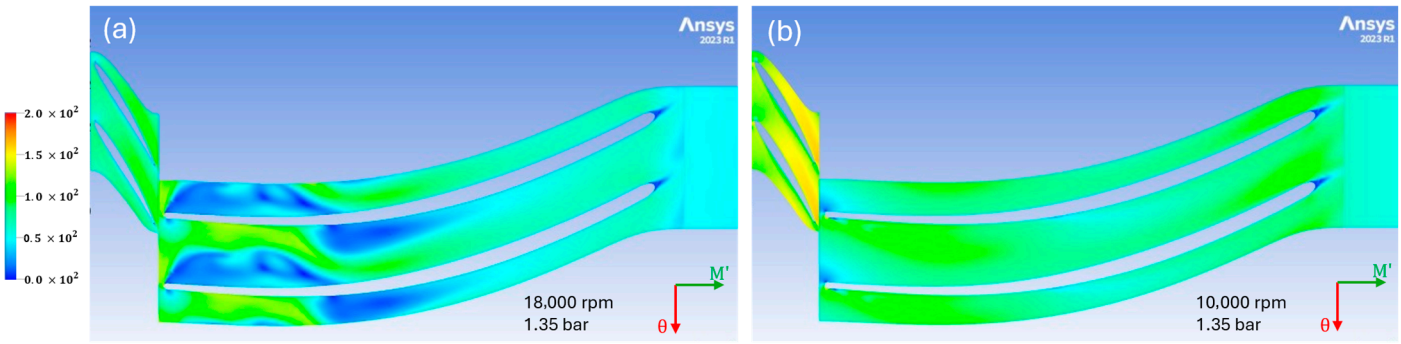


Figure 7. Isosurface (span position = 0.5) view of the radial turbine. (**a**) Rotational speed of 18,000 rpm. (**b**) Rotational speed of 10,000 rpm.

In this system, the turbine operating point is largely dictated by the outlet temperature requirement, and the total available pressure drop. Since the system requires a nearly constant mass flow rate, reduced pressure ratios must be compensated by a corresponding reduction in shaft speed. This ensures that the turbine continues to operate within a favourable range of its characteristic map. Figure 7 clearly illustrates this relationship: at a fixed pressure of 1.35 bar, a lower rotational speed aligns the turbine's flow capacity with the system demand.

Overall, stable operating points can be identified by a combination of factors: smooth trends in the performance curves, an absence of flow separation in the velocity field, and a consistent solver convergence. Performance maps offer a macroscopic view of efficiency trends and power output, while CFD post-processing reveals local flow phenomena such as backflow, tip leakage, or unsteady blade loading. Both perspectives are essential to ensure reliable and safe turbine operation over the full range of off-design conditions.

3.2. Operation Map—Air Cycle

The operating behaviour of the air cycle machine can be divided into three characteristic zones, each dominated by different component dynamics. At low outlet temperatures, the turbine performance is the governing factor. In contrast, at high outlet temperatures, the compressor behaviour becomes dominant. Between these two regimes lies a transitional region in which both the turbine and compressor contribute to performance, but neither operates at a full capacity.

As shown in Figure 8 the system's control strategy adapts to the temperature set-point. At low temperature targets (e.g., below 0 °C), the turbine operates near its optimal efficiency line, as shown in Figure 6 and the compressor speed is reduced to balance the

mass flow. The turbine absorbs the available pressure drop, and cooling is primarily achieved through energy extraction. As the outlet temperature increases and approaches 0 °C, the system enters a transition region where the turbine is progressively bypassed using the bypass valve. Once the turbine is fully bypassed, a further temperature increase is achieved by throttling the chiller. Eventually, to reach high temperature targets (e.g., above 80–100 °C), the compressor must increase its rotational speed, generating the required pressure difference. At these conditions, the turbine remains bypassed and the chiller is inactive. The pressure build-up is then managed by adjusting the outlet valve to maintain system pressure stability.

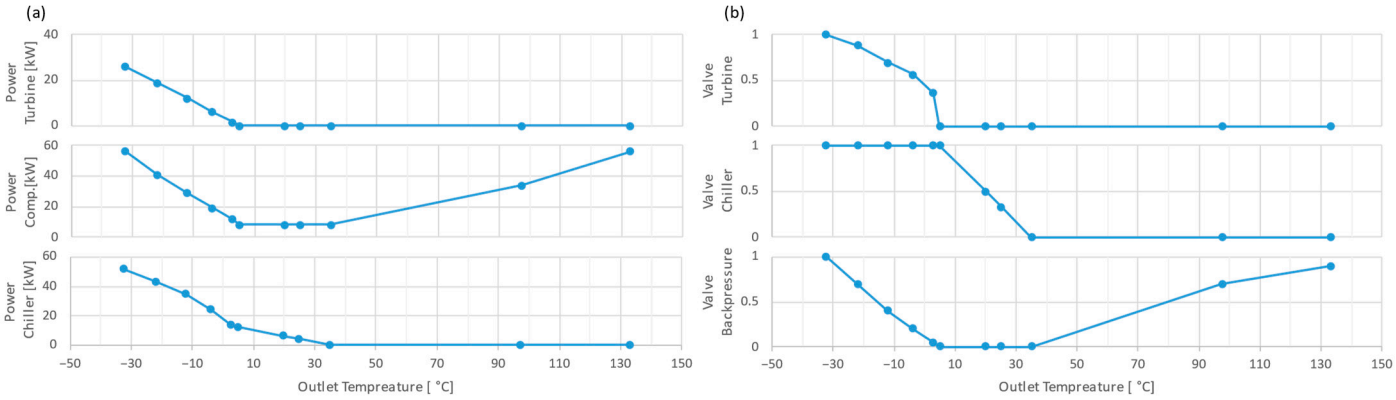


Figure 8. (**a**,**b**) Approximated operating strategy of the main components.

This strategy enables a wide operational temperature range, from approximately −30 °C with the turbine running at full power and maximum chiller capacity to over 130 °C with the compressor operating at full speed and all cooling elements bypassed.

The overall control system combines set-point scheduling with gain-scheduled PID loops. A supervisory layer classifies the operating regime and retrieves base set-points for the compressor speed, turbine bypass position, and outlet pressure valve from lookup tables as a function of the requested outlet temperature and pressure. Because temperature dynamics are slow, the loops are arranged in a cascade as shown in Figure 9. Fast inner loops regulate outlet pressure and shaft speeds, while a slower outer loop regulates outlet temperature by biassing the inner-loop set-points. A fuzzy gain-scheduling block [35–38] refines the scheduled gains and applies small adaptive corrections to the set-points in real time using error and error-rate information. The fuzzy scheduler works alongside the lookup tables in the supervisor, providing adaptivity without sacrificing the stability of the base tuning.

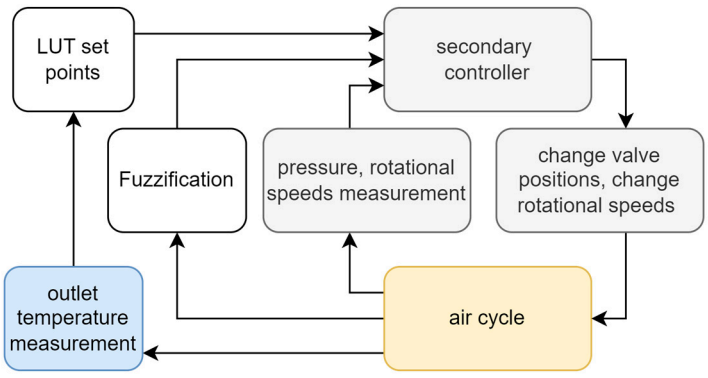


Figure 9. Cascade control system. Outer loop measuring temperature; inner loop measuring rotational speeds and pressure levels. Fuzzification dynamically adapts the control parameters while the outer LUT predefines the zone and initial values.

By combining component performance maps with rule-based control and adaptive feedback loops, the system ensures a robust and flexible operation across a wide temperature spectrum. Each region of the operation map demands a tailored control approach, reinforcing the need for coordinated controller design and system-level tuning.

4. Discussion

Recent regulatory developments in the automotive industry demand significant adaptations of the existing test infrastructure. This work introduces a novel air conditioning system designed to meet these challenges by expanding the capabilities of dynamometer test benches through the application of an innovative air cycle concept. Unlike conventional thermal conditioning systems, the proposed design leverages low thermal mass and highly dynamic turbomachinery to enable the fast and precise control of the air conditions.

The system architecture—with separate compressor and turbine units and a chiller that can be partially or fully bypassed—permits a wide and flexible operating range. As demonstrated, the unit can simulate ambient conditions spanning from the high temperatures of summer to the freezing cold of Nordic winters. Through active pressure control at the outlet, airflow and pressure profiles can be adjusted to replicate both lowland and high-altitude environments. This level of environmental flexibility significantly extends the realistic testing capabilities of the current powertrain and battery testing platforms.

Beyond the hardware, this work also provides insights into a modular open source software framework for turbomachinery design and simulation. The pyNURBS module enables flexible low-level CAD modelling, while pyTurbo provides a structured approach to the aerodynamic and thermodynamic design of turbomachinery components. The software tools were successfully integrated into a simulation workflow using standard industry tools such as Ansys CFX, supporting geometry generation, meshing, and performance evaluation.

It is important to emphasise that the system's operational logic and control strategy are currently based on numerically derived performance maps. While the simulation results provide a strong foundation, experimental validation and refinement of the control system are essential in subsequent development stages. Particular attention must be paid to transient phenomena during turbine bypass activation, as controller smearing effects may introduce instability or overshoot. In addition, potential instability zones in turbine operation—highlighted during the off-design analysis—must be confirmed and monitored during commissioning. Fine-tuning of the PID and lookup-based control layers, especially near transition zones, will be crucial for robust real-world operation.

Author Contributions: L.H.: writing—review and editing, writing—original draft, validation, software, methodology, conceptualization. Z.R.: writing—review and editing, supervision, Software. M.T.: methodology. All authors have read and agreed to the published version of the manuscript.

Funding: The authors would like to acknowledge the support provided by the Austrian Research Promotion Agency (FFG) through grant FO999896814. This project is conducted in collaboration between Montanuniversität Leoben and Christof Systems GmbH.

Data Availability Statement: The datasets presented in this article are not readily available because the data are part of an ongoing.

Conflicts of Interest: Author Michael Tielsch was employed by the company Christof Systems GmbH. The remaining authors declare that the research was conducted in the absence of any commercial or financial relationships that could be construed as a potential conflict of interest.

Abbreviations

The following abbreviations are used in this manuscript:

Symbols

p	Pressure (Pa)	κ	Heat capacity ratio (-)
T	Temperature (K)	c_p	Heat capacity (J/kg·K)
$p01$	Total pressure at the outlet (Pa)	π	Pressure ratio (-)
$p5$	Static pressure at the outlet (Pa)	P	Power (W)
$\dot{m}$	Mass flow (kg/s)	N	Revolutions (rpm)
C_Θ	Tangential velocity (m/s)	U	Blade speed (m/s)
η	Efficiency (-)	$\dot{V}$	Volume flow (m^3/h)
h	Specific enthalpy (J/kg)	x	Valve position (-)
W	Work (W)	Q	Heat flux (W)
n_t, n_c	Polytropic coefficient turbine compressor		

Abbreviations

NURBS	Non-uniform rational B-Splines	RDE	Real Driving Emission
FEM	Finite elements method	WLTP	World-harmonized Light-duty Vehicles Test Procedure
CAD	Computer-aided design	COP	Coefficient of Performance
CFD	Computer fluid dynamics	APU	Auxiliary Power Unit
PID	Proportional–integral–derivative controller	PPA	Projected Polyhedron Algorithm
VCRS	Vapour compression refrigeration system	RANS	Reynolds-Averaged Navier–Stokes
GWP	Global warming potential	rpm	Revolutions per minute
		SST	Shear stress transport

References

1. European Environment Agency. Greenhouse Gas Emissions from Transport in Europe. 2023. Available online: https://www.eea.europa.eu/en/analysis/indicators/greenhouse-gas-emissions-from-transport?activeAccordion=546a7c35-9188-4d23-94ee-005d97c26f2b (accessed on 15 April 2024).
2. Air Quality Expert Group. Non-Exhaust Emissions from Road Traffic. 2019. Available online: http://uk-air.defra.gov.uk (accessed on 11 April 2024).
3. Giechaskiel, B.; Grigoratos, T.; Dilara, P.; Karageorgiou, T.; Ntziachristos, L.; Samaras, Z. Light-Duty Vehicle Brake Emission Factors. *Atmosphere* **2024**, *15*, 97. [CrossRef]
4. Fussell, J.C.; Franklin, M.; Green, D.C.; Gustafsson, M.; Harrison, R.M.; Hicks, W.; Kelly, F.J.; Kishta, F.; Miller, M.R.; Mudway, I.S.; et al. A Review of Road Traffic-Derived Non-Exhaust Particles: Emissions, Physicochemical Characteristics, Health Risks, and Mitigation Measures. *Environ. Sci. Technol.* **2022**, *56*, 6813–6835. [CrossRef] [PubMed]
5. Dornoff, J.; Rodríguez, F. Euro 7: The New Emission Standard for Light-and Heavy-Duty Vehicles in the European Union. 2024. Available online: https://theicct.org/wp-content/uploads/2024/03/ID-116-%E2%80%93-Euro-7-standard_final.pdf (accessed on 8 August 2025).
6. GRPE. Euro 7 New Proposal for Vehicle Emissions Type Approval in Europe (GRPE 87). 2023. Available online: https://unece.org/transport/events/wp29grpe-working-party-pollution-and-energy-87th-session (accessed on 13 April 2024).
7. Publications Office of the EU. *Euro 7 Impact Assessment Study*; Publications Office of the EU: Luxembourg, 2022. [CrossRef]
8. Mathissen, M.; Grochowicz, J.; Schmidt, C.; Vogt, R.; zum Hagen, F.H.F.; Grabiec, T.; Steven, H.; Grigoratos, T. A novel real-world braking cycle for studying brake wear particle emissions. *Wear* **2018**, *414*, 219–226. [CrossRef]
9. Bondorf, L.; Köhler, L.; Grein, T.; Epple, F.; Philipps, F.; Aigner, M.; Schripp, T. Airborne Brake Wear Emissions from a Battery Electric Vehicle. *Atmosphere* **2023**, *14*, 488. [CrossRef]
10. Hesse, D.; Augsburg, K.; Feißel, T. Real Driving Emissions Measurement of Brake Dust Particles. 2019. Available online: https://www.researchgate.net/publication/334671579 (accessed on 5 July 2025).
11. Huber, M.P.; Fischer, P.; Mamakos, A.; Steiner, G.; Klug, A. Measuring Brake Wear Particles with a Real-Driving Emissions Sampling System on a Brake Dynamometer. In *SAE Technical Papers*; SAE International: Warrendale, PA, USA, 2022.

12. Niemann, H.; Winner, H.; Asbach, C.; Kaminski, H.; Frentz, G.; Milczarek, R. Influence of disc temperature on ultrafine, fine, and coarse particle emissions of passenger car disc brakes with organic and inorganic pad binder materials. *Atmosphere* **2020**, *11*, 1060. [CrossRef]
13. GRPE. *Proposal for a New UN GTR on Laboratory Measurement of Brake Emissions for Light-Duty Vehicles (ECE/TRANS/WP.29/2023/79)*; GRPE: Geneva, Switzerland, 2023.
14. Hammerschmidt, L.; Tielsch, M.; Spijker, C. Process air conditioning—The transition to air cycles in the automotive and mobility test infrastructure. In Proceedings of the Deutsche Kälte- und Klimatagung 2023, Hannover, Germany, 22–24 November 2023.
15. Hammerschmidt, L. Development of a Radial Inflow Turbine for Sub-Zero Applications on an Automotive Dynamometer. Master's Thesis, Montanuniversität Leoben, Leoben, Austria, 2020.
16. Airtech AKB Series, AIRTECH Group Inc. Available online: https://www.airtechusa.com/media/AKB1000-Series-2020.pdf (accessed on 23 October 2025).
17. Aungier, R.H. *Turbine Aerodynamics: Axial-Flow and Radial-Flow Turbine Design and Analysis*; ASME Press: New York, NY, USA, 2006. [CrossRef]
18. Hammerschmidt, L.; Roanic, Z. Enhanced Turbomachinery Capabilities for OpenFOAM: Validation and Integration of a CAD Solution and Mixing-Plane. *Int. J. Thermofluids* **2025**, *2*, 101341. [CrossRef]
19. Patrikalakis, N.M.; Maekawa, T.; Ko, K.H.; Mukundan, H. Surface to Surface Intersections. *Comput.-Aided Des. Appl.* **2004**, *1*, 449–457. [CrossRef]
20. Patrikalakis, N.M.; Maekawa, T. *Shape Interrogation for Computer Aided Design and Manufacturing*; Springer: Berlin/Heidelberg, Germany, 2010. [CrossRef]
21. Lee, H.G.; Shin, J.H.; Choi, C.-H.; Jeong, E.; Kwon, S. Partial admission effect on the performance and vibration of a supersonic impulse turbine. *Acta Astronaut.* **2018**, *145*, 105–115. [CrossRef]
22. Alshammari, F. Radial Turbine ExpanderDesign, Modelling and Testing for Automotive Organic Rankine Cycle Waste Heat Recovery. Ph.D. Thesis, Brunel University, London, UK, 2018.
23. Beaudoin, M.; Nilsson, H.; Page, M.; Magnan, R.; Jasak, H. Evaluation of an improved mixing plane interface for OpenFOAM. In *IOP Conference Series: Earth and Environmental Science*; Institute of Physics Publishing: Montreal, QC, Canada, 2014. [CrossRef]
24. Hanimann, L.; Mangani, L.; Casartelli, E.; Mokulys, T.; Mauri, S. Development of a novel mixing plane interface using a fully implicit averaging for stage analysis. *J. Turbomach.* **2014**, *136*, 081010. [CrossRef]
25. Gisbert, F.; Corral, R. A Novel mixing plane method using nonreflecting boundary conditions for multirow analysis in turbomachines. *J. Turbomach.* **2016**, *138*, 071009. [CrossRef]
26. Cvijetić, G.; Jasak, H. Harmonic Balance Method for Turbomachinery Applications. In *OpenFOAM®*; Springer International Publishing: Cham, Switzerland, 2019; pp. 223–233. [CrossRef]
27. Oliani, S.; Casari, N.; Carnevale, M. A New Framework for the Harmonic Balance Method in OpenFOAM. *Machines* **2022**, *10*, 279. [CrossRef]
28. Hall, K.C.; Thomas, J.P.; Clark, W.S. Computation of Unsteady Nonlinear Flows in Cascades Using a Harmonic Balance Technique. *AIAA J.* **2002**, *40*, 879–886. [CrossRef]
29. Hanimann, L.; Mangani, L.; Casartelli, E.; Gröschel, E.; Fischer, M. Steady-state fluid-solid mixing plane to Replace transient conjugate heat transfer computations during design phase. *Int. J. Turbomach. Propuls. Power* **2021**, *6*, 6. [CrossRef]
30. Hoerner, S. Characterization of the Fluid-Structure Interaction on a Vertical Axis Turbine with Deformable Blades. Available online: https://theses.hal.science/tel-02895310 (accessed on 8 June 2025).
31. Gadda, A.; Mangani, L.; Romanelli, G.; Mantegazza, P.; Casartelli, E. A GPU-accelerated compressible RANS solver for Fluid-Structure Interaction simulations in turbomachinery. In Proceedings of the International Symposium on Transport Phenomena and Dynamics of Rotating Machinery, ASME, 2016, Honolulu, HI, USA, 10–15 April 2016. Available online: https://hal.science/hal-01890058 (accessed on 9 June 2025).
32. Rogo, C.; Hajek, T.; Chen, A.G. *Variable Stator Radial Turbine*; NASA: Washington, DC, USA, 1984.
33. Okazaki, Y.; Matsuo, E.; Matsudaira, N.; Busch, P. Development of a variable area radial turbine for small turbochargers. In *Proceedings of the ASME Turbo Expo*; American Society of Mechanical Engineers: New York, NY, USA, 1988; Volume 2. [CrossRef]
34. Binder, N.; Le Guyader, S.; Carbonneau, X. Analysis of the variable geometry effect in radial turbines. *J. Turbomach.* **2011**, *134*, 041017. [CrossRef]
35. PROF. DIPL.-ING. PETER F. ORLOWSKI: Prozessoptimierung ohne Reglerparameter Die FRt-Wurzelrekursion. Technische Hochschule Mittelhessen. Available online: https://www.thm.de/me/images/user/orlowski-50/Prozessoptimierung-ohne-Parameter.pdf (accessed on 25 May 2025).
36. Orlowski, P.F. *Praktische Regeltechnik*; Springer: Berlin/Heidelberg, Germany, 2008. [CrossRef]

37. Li, P.; Irwin, G.W.; Kruger, U. A recursive rule base adjustment algorithm for a fuzzy logic controller. *Fuzzy Sets Syst.* **2005**, *156*, 267–284. [CrossRef]
38. Sun, Y.L.; Er, M.J. Design of a recursive fuzzy controller with nonlinear fuzzy rule base. In Proceedings of the 7th International Conference on Control, Automation, Robotics and Vision, 2002, ICARCV 2002, Marina Mandarin, Singapore, 2–5 December 2002; pp. 1574–1578. [CrossRef]

Disclaimer/Publisher's Note: The statements, opinions and data contained in all publications are solely those of the individual author(s) and contributor(s) and not of MDPI and/or the editor(s). MDPI and/or the editor(s) disclaim responsibility for any injury to people or property resulting from any ideas, methods, instructions or products referred to in the content.